Earth and Planetary Science Letters 304 (2011) 85–92

Contents lists available at ScienceDirect

Earth and Planetary Science Letters

journal homepage: www.elsevier.com/locate/epsl

Paleo-erosion rates in Central Asia since 9 Ma: A transient increase at the onset of Quaternary glaciations?

J. Charreau [a,*,1], P.-H. Blard [a,1], N. Puchol [a,1], J.-P. Avouac [b,2], E. Lallier-Vergès [c], D. Bourlès [d], R. Braucher [d], A. Gallaud [c], R. Finkel [d,e], M. Jolivet [f], Y. Chen [c], P. Roy [a]

[a] Centre de Recherche Pétrographique et Géochimique, 15 rue Notre Dame des Pauvres, B.P. 20, 54501 Vandoeuvre lès Nancy, France
[b] Tectonics Observatory, California Institute of Technology; Mail Code 100–23, Pasadena CA 91125, United States
[c] Institut des Sciences de la Terre d'Orléans; Bâtiment Géosciences, rue de Saint Amand, BP 6759, 45067 Orléans Cedex 2, France
[d] Centre Européen de Recherche et d'Enseignement des Géosciences de l'Environnement, Europole Méditerranéen de l'Arbois BP 80 13545 Aix-en-Provence Cedex 4, France
[e] Earth and Planetary Science Department, University of California, Berkeley, Berkeley CA, United States
[f] Géosciences Rennes (UMR CNRS 6118), Université de Rennes1, Bâtiment 15, Campus de Beaulieu, CS 74205, F-35042 Rennes Cedex, France

ARTICLE INFO

Article history:
Received 6 December 2010
Received in revised form 18 January 2011
Accepted 18 January 2011
Available online 20 February 2011

Editor: T.M. Harrison

Keywords:
Quaternary glaciation
erosion rates
Tianshan
cosmogenic nuclide
magnetostratigraphy
^{10}Be

ABSTRACT

Erosion is a fundamental player of the interactions existing between internal geodynamics and climate, in particular through its influence on the carbon dioxide budget. However, long term (>1 Ma) erosion rates, estimated indirectly from sediment budget, remain poorly constrained. While some studies suggest that worldwide erosion rates increased at the Plio-Pleistocene climatic transition (~4–2 Ma), the validity of this observation and its significance is a matter of debate due to potential biases of the sedimentary record and to the influence of sea level fall on the global sedimentary flux to marginal basins. In the present study, we estimate erosion rates over the last ~9 Ma using in situ produced cosmogenic ^{10}Be concentrations measured in magnetostratigraphically dated continental sediments. We focus on an intracontinental endorheic watershed draining the northern Tianshan in Central Asia, a key region regarding the ongoing debate. While erosion rates between 0.1 and 1 mm·yr^{-1} are derived from most of our record, they reach values as high as ~2.5 mm·yr^{-1} from 2.5 to 1.7 Ma. Then, after 1.7 Ma, recent and modern erosion rates fell below 1 mm·yr^{-1}. This temporary increase is correlated with the onset of Quaternary ice ages and suggests that global climate had a significant and transient impact on erosion.

1. Introduction

Erosion is a key factor governing the evolution of the Earth's surface evolution and provides a source of multiple feedback mechanisms linking climate and tectonics (France-Lanord and Derry, 1997; Molnar, 2004; Raymo and Ruddiman, 1992). First, erosion controls mass transfer from uplifting highlands. The ensuing redistribution of mass influences isostatic compensation in a way that induces tectonic deformation (Dahlen and Suppe, 1988; Whipple and Meade, 2006; Willett and Brandon, 2002). The resulting vertical movement of mass affects the thermal structure of the crust and hence its rheology (Avouac and Burov, 1996; Zeitler et al., 2001). Second, erosion is considered as a first order driving mechanism of the Earth's climate at the geological time scales because of its potential impact on atmospheric CO_2 through the creation of new surfaces enabling silicate weathering (Berner et al., 1983) but also because of its influence on the mechanical burial of organic carbon (Galy et al., 2007). Quantitative records of past erosion rates over geological time scales are thus of major importance to untangle the complex interactions between tectonics, climate and surface processes. Importantly, records of erosion rate over the last 10 Ma are crucial for addressing the respective causes and effects of glacial cycles that were initiated at the Cenozoic–Quaternary boundary.

Some authors (Molnar, 2004; Zhang et al., 2001) have reported a worldwide acceleration in accumulation rates at the Plio-Pleistocene transition (2–4 Ma) (Fig. 1) that they link to enhanced erosion. This finding, which suggests a major influence of Quaternary glaciation on global erosion rates, has recently been questioned on the ground of a new global ^{10}Be/^{9}Be record (Willenbring and von Blanckenburg, 2010). Interpreted as a proxy of continental weathering, this ratio has remained nearly constant over the last 12 Ma which led Willenbring and von Blanckenburg (2010) to conclude that the global Quaternary cooling

* Corresponding author. Tel.: +33 383594227; fax: +33 383511798.
E-mail addresses: charreau@crpg.cnrs-nancy.fr (J. Charreau), blard@crpg.cnrs-nancy.fr (P.-H. Blard), puchol@crpg.cnrs-nancy.fr (N. Puchol), avouac@gps.caltech.edu (J.-P. Avouac), elisabeth.verges@univ-orleans.fr (E. Lallier-Vergès), bourles@cerege.fr (D. Bourlès), braucher@cerege.fr (R. Braucher), audrey.gallaud@gmail.com (A. Gallaud), finkel@cerege.fr (R. Finkel), marc.jolivet@univ-rennes1.fr (M. Jolivet), Yan.Chen@univ-orleans.fr (Y. Chen), Pierre.Roy@etudiant.ensg.inpl-nancy.fr (P. Roy).
[1] These authors contributed equally to this work.
[2] Tel.: +1 626 395 4239; fax: +1 626 395 1740.

0012-821X/$ – see front matter © 2011 Elsevier B.V. All rights reserved.
doi:10.1016/j.epsl.2011.01.018

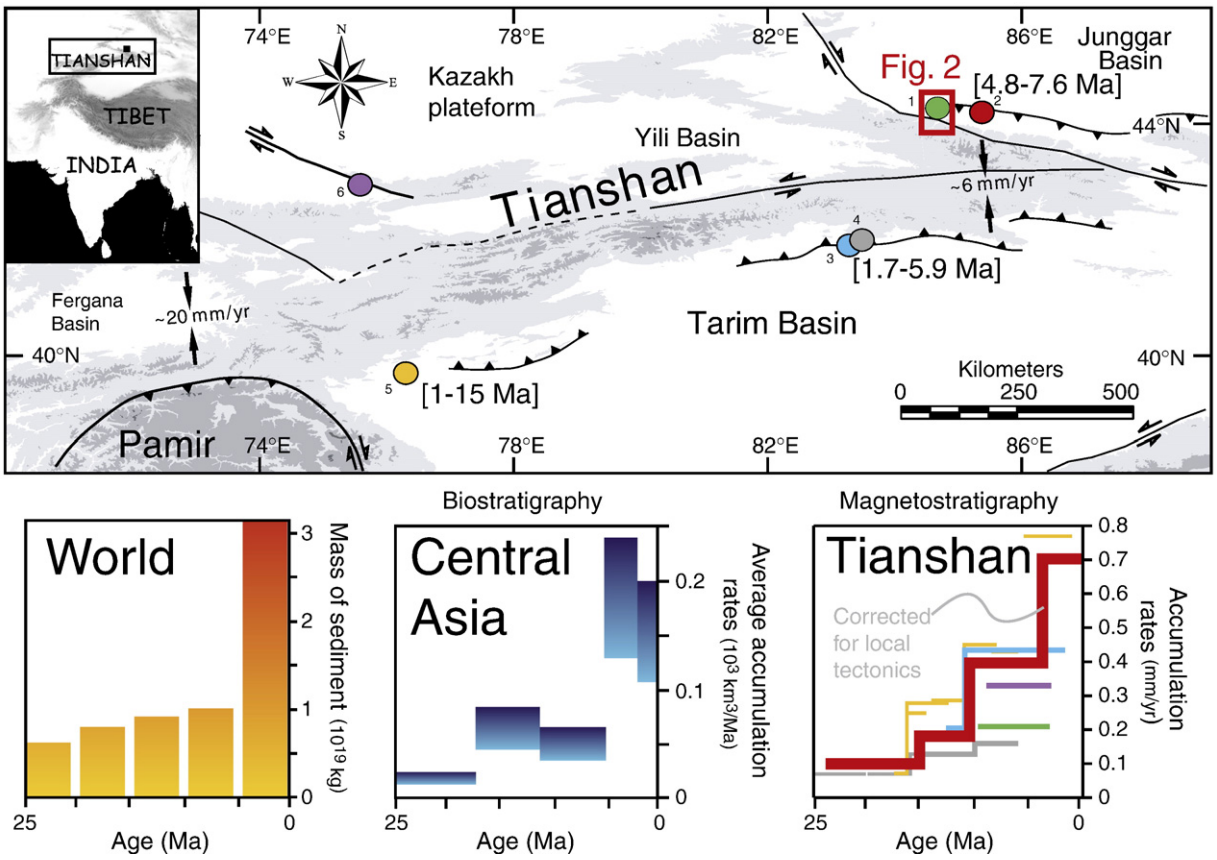

Fig. 1. Sediment flux and accumulation rates in Central Asia basins over the last 25 Myr. Topographic map of Central Asia with locations of all accumulation rate records derived from magnetostratigraphy in this region (see references in Charreau et al., 2009b). The basal age of the conglomeratic 'Xiyu' formation found at each of these locations is indicated in bracket (see references in Charreau et al., 2009b). At the bottom, from left to right, the evolution of sediment flux to basins for the world (Zhang et al., 2001), and Central Asia (Métivier and Gaudemer, 1997) and the accumulation rate records derived from magnetostatigraphy around the Tianshan (see references in Charreau et al., 2009b). The red box shows the location of Figure 2.

had no profound effect on global weathering rates. Moreover, erosion rates derived from sediment budgets suffer from drawbacks and potential flaws due to uncertainties on depositional ages in intracontinental areas (Charreau et al., 2009b), poor constraints on basin geometry (Clift, 2006) and inaccurate volume reconstruction methods (Métivier, 2002). Furthermore, the global sediment budget might actually be biased by the effect of the sea level drop during glacial times that remobilized loose sediments previously stored on the continental margins (Hay et al., 1988). Finally, the Quaternary increase of local accumulation rates could reflect an observational artifact, due to the increasing likelihood that sedimentary deposits will have been lost with the increasing age of the deposit (Sadler, 1999).

Central Asia stands out as a key area with regard to this debate. Indeed, because of its intracontinental endorheic setting, the sediment budget in this region is insensitive to global sea-level variations and can be constrained reasonably well from the closed basins systems (Fig. 1). The large Pleistocene increase of sediment flux to the basins reported in previous studies (Métivier and Gaudemer, 1997; Zhang et al., 2001) is therefore a key observation. However, these observations are also prone to hiatus artifacts and they relied heavily on the assumption that the widely distributed conglomeratic units, often referred to the Xiyu Formation, were regionally synchronous. Several magnetostratigraphic studies (Charreau et al., 2009b; Heermance et al., 2007) have however shown that the onset of formation of the Xiyu conglomerates is, in fact, diachronous, with ages ranging between 1 and 15 Ma (Fig. 1). Moreover, accumulation rates derived from these studies (Fig. 1) yield widely varying results for the 0–5 Ma period, probably because of tectonics modulation on the available space in the piedmont (Charreau et al., 2008).

In situ produced cosmogenic nuclide concentration in river sediments allow the derivation of average erosion rates within a given watershed (Brown et al., 1995, 1998), because at steady state, the nuclide concentration is inversely proportional to the denudation rate and because the river sediments have moreover the remarkable property to provide a spatially averaged erosion rate for the whole drainage basin (von Blanckenburg, 2005). This method has been successfully applied to determine erosion rates in a broad range of modern (von Blanckenburg, 2005) and relatively recent (less than ~1 Ma old) environments (Blard et al., 2006; Schaller et al., 2002). So far, only Refsnider (2010) using cosmogenic analysis of cave sediments has provided an estimate of erosion rate since 5 Ma, in the Rocky Mountains.

Here, we expand the method to longer geological records to infer erosion rates by measuring the fossil in situ produced cosmogenic signal in buried sediments along a magnetostratigraphically dated section (Charreau, 2005) from the North Tianshan Piedmont in Central Asia (Figs. 1 and 2). This record spans from 9 Ma to the present, a time period that is particularly relevant to address the feedbacks between long-term global climate, tectonics and erosion. This study moreover demonstrates the possibility of estimating past erosion rates combining cosmogenic analyses with magnetostratigraphic dating of sediments.

2. Geological settings and sampling

We analyze sediments from the Kuitun river watershed which drains the northern Tianshan shedding sediments to the Junggar foreland basin (Figs. 1 and 2). The Tianshan is a 2500-km-long

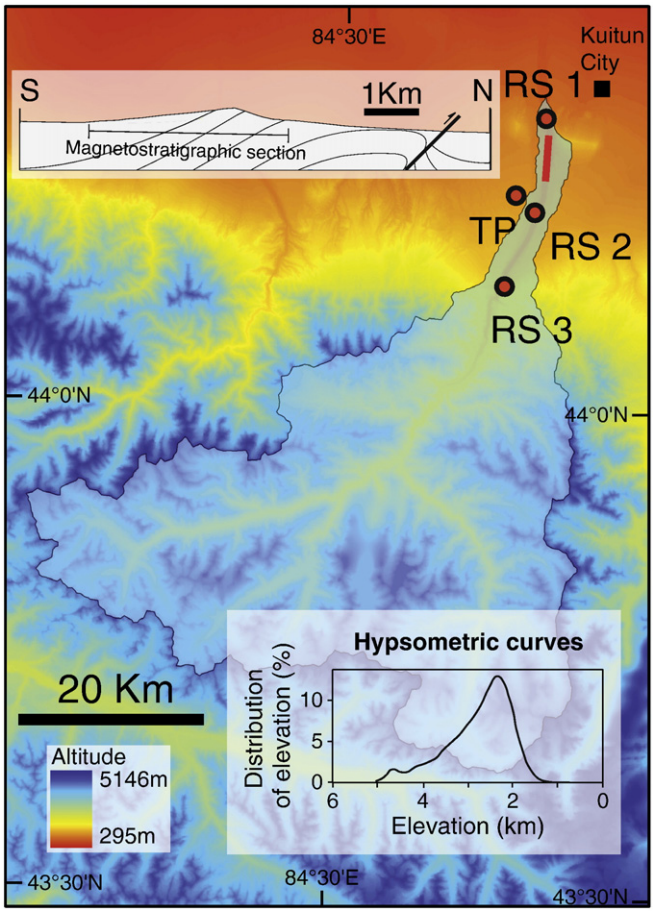

Fig. 2. Geographic and stratigraphic setting of the samples. Map of the Kuitun river's watershed area with location of the river sands (RS) and terrace profile (TP) cosmogenic samples. Red line AA' shows location of the magnetostratigraphic section where samples were also collected for cosmogenic analysis. Top: structural cross section of the Dushanzi anticline and extent of the magnetostratigraphic section. Right: magnetostratigraphic column of the Kuitun section and its correlation to the polarity reference scale with red stars indicating the stratigraphic position of the samples collected for cosmogenic analysis.

tectonically active mountain range that dominates Central Asia with an average altitude of 2500 m and summits reaching up to 7000 m. While its geology consists of mainly island arc rocks linked to a long-lived Paleozoic history of subduction/collision (Burtman, 1975; Charvet et al., 2007; Gao et al., 1998; Lin et al., 2008; Wang et al., 2008; Windley et al., 1990), the present high topography attests to a more recent and intense deformation. This later owes its origin to the Cenozoic reactivation of the range during the Oligocene to early Miocene (>16 Ma) (Avouac et al., 1993; Bullen et al., 2001, 2003; Charreau et al., 2005, 2006, 2009a; Dumitru et al., 2001; Sobel and Dumitru, 1997; Sobel et al., 2006; Windley et al., 1990; Yin et al., 1998), under the influence of the ongoing India–Asia collision. The Tianshan range indeed plays a major role in the India–Asia collision since it presently accommodates up to 40% of the total convergence between those two continents (Abdrakhmatov et al., 1996; Reigber et al., 2001). It is sandwiched between two large intracontinental basins (Fig. 1) filled by the eroded materials shed from the uplifting range. In the piedmonts, tectonic wedges constituted of numerous fold and thrust belts have overthrusted Lower Mesozoic to Quaternary sediments that were initially deposited in the foreland basin. Thanks to strong Holocene river entrenchment (Poisson and Avouac, 2004) into these piedmont fold-and-thrust belts, several exceptional sections are well exposed and now enable high resolution analysis of this thick and continuous sedimentary records.

Our study focuses on the 1.8-km-thick Kuitun section that is located near the Dushanzi city, 300 km west of Urumqi (Fig. 2). This location is very suitable because cosmogenic production due to recent exposure can be accurately quantified (Poisson and Avouac, 2004) and because depositional ages are independently well constrained by a magnetostratigraphic analysis (Charreau et al., 2005) that yielded ages from ~10.5 to ~1.5 Ma (Fig. 3). Magnetostratigraphic dating also permitted these authors to constrain the sediment accumulation rates between 0.12 and 0.46 mm/yr. This constraint is fundamental to estimate the cosmogenic production during sediment burial (see below).

Seventeen sandstone samples were collected along the freshly exposed outcrop of this Cenozoic section(Fig. 2), as well as three modern sands from the Kuitun river bed and a 150-cm-thick profile from a 15 ± 3 ka terrace (Molnar et al., 1994; Poisson and Avouac, 2004) (Fig. 2).

3. Methods and measurements

3.1. Cosmogenic isotopes in modern river sediments

At a single location i, in surficial rocks undergoing continuous thin-layers removal by erosion, the concentration (atom·g^{-1}) of cosmogenic isotopes N_i (e.g. ^{10}Be), is expressed by the following equation (Lal, 1991):

$$\varepsilon_i = \frac{\Lambda}{\rho}\left(\frac{P_i}{N_i} - \lambda\right), \quad (1)$$

where P_i (atom g^{-1} a^{-1}) is the surface production rate, Λ (g·cm^{-2}) the attenuation length, λ (a^{-1}) the radioactive decay constant of the nuclide, ε (cm·yr^{-1}) the erosion rate and ρ (g·cm^{-3}) the density. It must be noted that this equation is valid only if the surface exposure time is sufficiently long (i.e. $t >> 1/(\lambda + \varepsilon\rho/\Lambda)$ to have reached steady state and if the inherited cosmogenic concentration can be neglected.

Importantly, the cosmogenic nuclide concentration measured in river sands has the remarkable property of averaging the concentration of all surficial rocks outcropping in the drainage basin (Brown et al., 1995; von Blanckenburg, 2005). It is thus possible to determine the average erosion rate $\overline{\varepsilon}$ for a whole drainage basin by measuring the mean cosmogenic nuclide concentration $\overline{N}$ in river sand. Eq. (1) requires calculation of the average production rate $\overline{P}$ at the surface in the drainage basin. The modern production rate was calculated here using the present day watershed hypsometry by combining the S.R.T.M. (Shuttle Radar Topography Mission) D.E.M. (Digital Elevation Model) of the Kuitun watershed (Fig. 2) along with the geological map to precisely identify the altitude of quartz rock sources. A scaling factor multiplying the sea level production rate is associated to each altitude. The arithmetic mean of these scaling factors is 9.5 ± 0.7 for the whole drainage. The scaling factor is 1.9 ± 0.2 at the location of the sediment deposition. These values are obtained using the scaling scheme of Lal/Stone (Lal, 1991; Stone, 2000). The topographic shielding was also considered using the S.R.T.M D.E.M and following Dunne et al. (1999).

3.2. Cosmogenic isotopes in buried sediments

Deriving erosion rates from cosmogenic isotopes in an old sedimentary sequence requires knowledge of: i) the age of deposition of the studied sedimentary archive, ii) the cosmogenic paleo-production rate of the whole drainage basin at the time of deposition and iii) the build-up of cosmogenic nuclides between the times of sediment deposition and sample collection (Fig. 4).

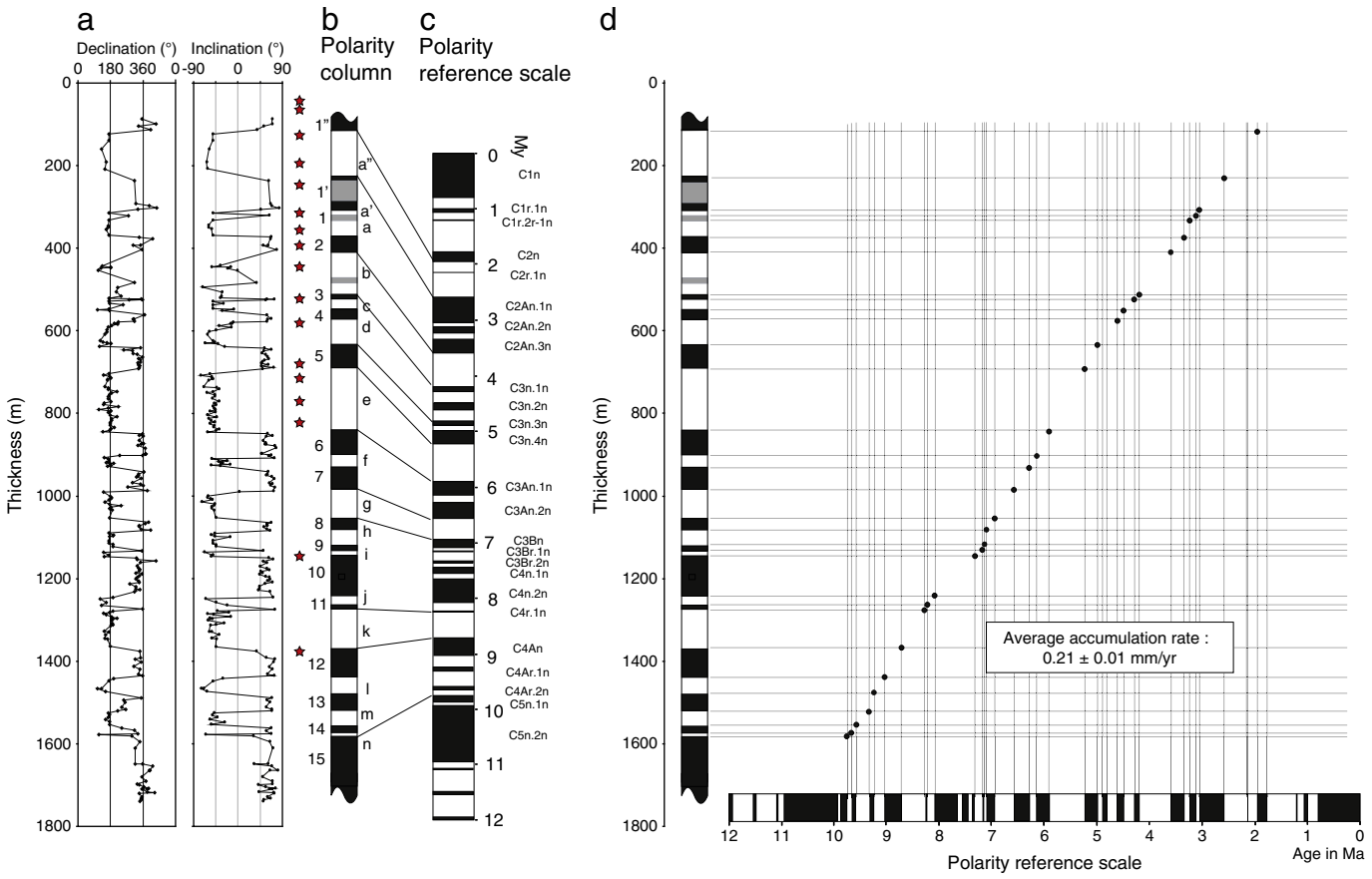

Fig. 3. Magnetostratigraphic analysis of the Kuitun section (after Charreau et al., 2005). (a) Magnetic declination and inclination measured in the Kuitun section. (b) Magnetostratigraphic column of the Kuitun section. Each normal (black) and reverse (white) polarity chron is defined by at least two samples from two different sedimentary horizons. Reversals found in a single bed are shown in gray. (c) Reference polarity time scale after Lourens et al. (2004); (d) age versus depth plot of the Kuitun section, using the data and correlation from 3b and 3c.

3.2.1. Estimation of the cosmogenic paleo-production rate

Recent analyses of pedogenetic carbonate in the same Kuitun section yielded constant $\delta^{18}O$ over the last 10 Ma, which suggests the hypsometry of the Kuitun drainage basin was relatively steady during this time (Kent-Corson et al., 2008). Moreover, given the relatively high latitude of the Kuitun watershed (45°N), time variations of the geomagnetic field (Biggin et al., 2009) induced cosmogenic production variations of less than 5% over the considered time period (last

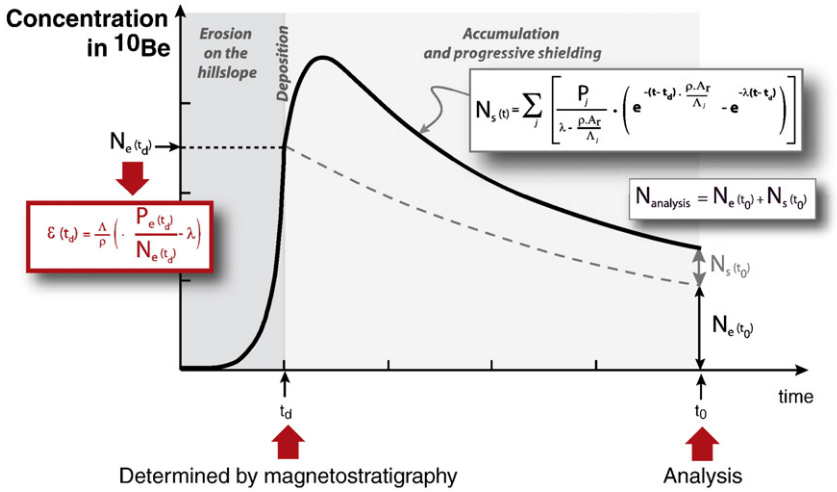

Fig. 4. Theoretical evolution of the ^{10}Be concentration in a quartz grain from its erosion on the hillslope to its deposition and burial in the foreland basin. The possible later phase of accumulation related to exhumation of the sample is not represented here. t_0: time of the analysis; t_d: time of deposition; $N_{analysis}$: concentration measured at a time t_0 in a given sediment sample (in $at \cdot g^{-1} \cdot yr^{-1}$); $N_s(t_0)$: concentration acquired during sediment burying minus the loss due to radioactive decay (in $at \cdot g^{-1} \cdot yr^{-1}$); $N_e(t_0)$: concentration acquired during the erosion minus the loss due to radioactive decay (in $at \cdot g^{-1} \cdot yr^{-1}$); $N_e(t_d)$: concentration acquired during the erosion on the drainage basin (in $at \cdot g^{-1} \cdot yr^{-1}$); A_r: accumulation rate (in $cm \cdot yr^{-1}$); P_j: the surface production rates by spallation, fast muons and slow muons captures (in $at \cdot g^{-1} \cdot yr^{-1}$) at the deposition location; λ: the radioactive decay constant (in yr^{-1}); ρ: the overlying sediment density (in $g \cdot cm^{-3}$); Λ_j: attenuation lengths ($g \cdot cm^{-2}$) of spallogenic and muogenic productions; $P_e(t)$: the average spallation production rate for the whole drainage basin (in $at \cdot g^{-1} \cdot yr^{-1}$); $\varepsilon(t_d)$: the erosion rates on the drainage basin at the time of deposition (in $cm \cdot yr^{-1}$).

10 Myr) (Dunai, 2001). Therefore, we assume that the paleo-production rate of ^{10}Be was similar to the modern rate. To take into account the weight of this assumption, we also propagated to the calculated erosion rates an uncertainty of 150 m attached to the catchment average elevation. This elevation uncertainty results from the standard deviation of the δ^{18}O record (Kent-Corson et al., 2008) considering that the δ^{18}O-altitude dependence is −2.8‰/km (Chamberlain and Poage, 2000).

3.2.2. Corrections of the post-depositional ^{10}Be accumulation

The ^{10}Be concentration analyzed in a given sample is the sum of the concentration inherited during the erosion on the hillslope plus that due to the post-depositional accumulation during burial and the accumulation during the modern exposure at the surface (Fig. 4). Therefore, to retrieve the true paleo-erosion rates one must correct the measured concentration from both the post-depositional and modern exposure accumulation.

When buried at a sufficient depth (~4 m), sediments are almost totally shielded from cosmic rays and, the radioactive cosmogenic nuclides consequently decay with time. In continental environments, the process of fluvial sediment deposition is in many cases too slow to provide an immediate shielding from cosmic rays. The ^{10}Be build-up during the progressive sediment burial can however be described by the following equation (Braucher et al., 2000):

$$N_{\text{shield}} = \sum_j \left[\frac{P_j}{\lambda - \frac{A_r \rho}{\Lambda_j}} \left(e^{-t\frac{A_r \rho}{\Lambda_j}} - e^{-\lambda t} \right) \right], \quad (2)$$

with P_j the surface production rates by spallation, by fast muons and by slow muon captures (in at.g^{-1}.yr^{-1}, see below), λ the radioactive decay constant (4.997×10^{-7} yr^{-1}) (Chmeleff et al., 2010), ρ the overlying sediment density (2.4 ± 0.13 g·cm^{-3}, determined from seismic speeds), A_r the accumulation rate (cm·yr^{-1}), Λ_j the typical attenuation lengths (g·cm^{-2}, see below) and t (yr) the time during which the sediment is getting buried.

To calculate the ^{10}Be production during the burial accumulation, the crucial parameter A_r was determined by using the high-resolution paleomagnetic record of Charreau et al. (2005). This magnetostratigraphic study constraints the accumulation rate at the time of deposition between 0.115 ± 0.006 and 0.418 ± 0.021 cm·yr^{-1}. The use of an 'instantaneous' accumulation rate (i.e. calculated for each magnetic chron) is justified for the spallation reactions from rapid neutrons because production by spallation is characterized by a short attenuation length (~160 g·cm^{-2}) (Lal, 1991), and becomes negligible below ~3 m. However, accumulation rate derived from magnetostratigraphy represent a long term (>20 Ka) average. Yet, in such continental and fluvial settings, rapid and short time scale variations in accumulation rate probably exist. Their potential impact on the cosmogenic building remains difficult to constrain and will be assumed negligible in this study. In future studies, complementary cosmogenic analysis will be required to test this assumption.

In contrast, the production by slow muon capture and fast muon reactions has a long attenuation length (respectively 5300 ± 950 g·cm^{-2} and 1500 ± 100 g·cm^{-2}) (Braucher et al., 2003) and remains significant for a long period of time even under several tens of meters of sediments. We therefore used an average accumulation rate of the whole sedimentary pile overlying each sample to correct for the post burial muonic production.

We used a sea level, high latitude surface production rate of 4.5 ± 0.3 at·g^{-1}·yr^{-1} (Amidon and Farley (2011) recalculated after Balco et al. (2008)). Both fast and slow muonic production were taken as $0.8 \pm 0.25\%$ (Braucher et al., 2003) of the total production rate at sea level, then scaled with the altitude following Stone (2000). Figure 4 shows the theoretical evolution of the cosmogenic concentration in a sedimentary material that has been successively eroded, transported and deposited. The present-day cosmogenic concentration $N_{\text{analysis}}(t_0)$ measured in a given sediment sample is the sum of $N_e(t_0)$, which represents the concentrations acquired during erosion and $N_s(t_0)$, which represents the concentration acquired during sediment burial (Fig. 4). Given the considered time-scales, both $N_e(t_0)$ and $N_s(t_0)$ may have undergone a significant radioactive decay since the initial ^{10}Be production (Blard et al., 2006). The possible later phase of accumulation during the recent exposure of the sample is not represented on Figure 4. Knowing independently the depositional age t_d and the accumulation rates A_r, Eq. (2) allows calculation of $N_s(t_0)$ and therefore $N_e(t_0)$. Then, knowing t_d, $N_e(t_0)$ can be directly corrected for the radioactive decay to calculate $N_e(t_d)$. Finally, $N_e(t_d)$ is converted into erosion rate $\varepsilon(t_d)$ at the time of deposition using Eq. (1).

It is important to note that the correction for production during sediment deposition is the major source of uncertainty of the paleo-erosion rates determined here. Indeed, when the ratio of erosion/accumulation is high (>>1), then the measured paleo-erosion rate is close to the detection limit of the method.

The sampled sediments were exposed during the Holocene incision of the Kuitun River at a rate constrained to 1 cm·yr^{-1}, by Optically Simulated Luminescence dating of terraces (Poisson and Avouac, 2004). Considering the present geometry of the Kuitun canyon at this location, this rate corresponds to a lateral cliff retreat of 3.5 cm·yr^{-1}. Due to this rapid incision, along with the topographic shielding of the cliff and a sampling strategy designed to ensure a current burial thickness of at least 1 m, the contribution of the modern exposure can be considered as negligible (i.e. 15 at.g^{-1}). It indeed ranges between less than 0.1% and 0.3% of the total present-day cosmogenic signal.

3.3. Samples treatment and measurement of ^{10}Be concentrations

Cosmogenic ^{10}Be concentration measurements were mainly performed at the French national AMS (Accelerator Mass Spectrometer) facility ASTER (Accelerator for Earth Sciences, Environment and Risks) located at the CEREGE laboratory (Aix en Provence, France) except for two samples, RS1 and TP, which were analyzed at the Center for Accelerator Mass Spectrometry at Lawrence Livermore National Laboratory in California (USA). All samples were crushed and the 200–500 μm fraction was treated as follows. Quartz was first enriched through successive magnetic separation, and flotation. Then, the enriched fraction was leached in H_2SiF6, HCl and HF to eliminate all remaining mineral phases but quartz and quartz surfaces were decontaminated from atmospheric ^{10}Be following the chemical procedures developed earlier (Brown et al., 1991). TP and RS1 were treated similarly but did not undergo flotation or H_2SiF_6 treatment. The purified quartz was then completely dissolved in HF after addition of 100 μl of an in-house $3.025\,10^{-3}$ g/g ^{9}Be carrier solution (in the case of TP and RS1 about 0.45 mg of a ^{9}Be carrier with a ^{10}Be blank of ^{10}Be/^{9}Be $= 6.7 \times 10^{-15}$ was used). Following subsequent purification by anion exchange, cation exchange and alkaline precipitations, purified beryllium oxide samples were analyzed on the AMS. ^{10}Be concentrations measured at ASTER are normalized to ^{10}Be/^{9}Be SRM 4325 NIST reference material with an assigned value of $(2.79 \pm 0.03) \times 10^{-11}$. This standardization is equivalent to 07KNSTD within rounding error. TP and RS1 were normalized to KNSTD3770 when they were measured in 1997 and were renormalized to 07KNSTD to take account of the KNSTD renormalization (Nishiizumi et al., 2007). The ^{10}Be half-life of $(1.39 \pm 0.01) \times 10^6$ yr used is that recently recommended by Chmeleff et al. (2010) and Korschinek et al. (2010) according to their two independent measurements. Measured ^{10}Be/^{9}Be blank ratios were $2.5 \pm 0.7 \times 10^{-15}$.

4. Results

All ^{10}Be results are presented in Table 1. In situ produced cosmogenic ^{10}Be concentrations measured in these samples range

between $(3.23\pm0.78)\times10^3$ and $(1.10\pm0.67)\times10^5$ at·g^{-1}. Erosion rates were calculated after correcting for the ^{10}Be radioactive decay and for the build-up of ^{10}Be during sediment accumulation following the methods presented above. Figure 5 shows the erosion rates plotted against the depositional ages along with the global deep-sea oxygen isotope records as a proxy for global climate (Zachos et al., 2001). Between 9 Ma and 3.5 Ma, erosion rates remained within 0.1 and 1 mm·yr^{-1}, with little fluctuations around an average value of 0.4 mm·yr^{-1} over that period of time. A significant sediment pulse characterized by erosion rates larger than 1 mm·yr^{-1} is evidenced between 3.5 Ma and 1.7 Ma, with a peak of 2.5 mm·yr^{-1} at 2 Ma. One additional sample (KBe12) from this time period (with age estimated to 2.1 Ma) is characterized by a low ^{10}Be concentration. Due to the supposed post-depositional correction, this precludes a precise estimation of erosion rates (see larges uncertainties in Table 1) for this sample. This is nevertheless consistent with the occurrence of very high (>2 mm·yr^{-1}) erosion rates over that period of time. After 1.5 Ma, the erosion rates dropped back to ~0.5 mm·yr^{-1}, a value consistent with the modern erosion rates of ~0.6 mm·yr^{-1} derived from the river sands and not significantly different from the value of 0.3 mm·yr^{-1} inferred from the Holocene (~15 ka) terrace material (Table 1).

5. Discussion and conclusion

This record shows a clear erosion pulse (from 3 to 1.7 Ma) that coincides with the onset of Quaternary glaciations as recorded by the global deep-sea oxygen isotope records (Zachos et al., 2001) (Fig. 5). Our data support the hypothesis that Quaternary glaciations were accompanied by a significant (>2 fold) increase of physical erosion rates in Central Asia, thereby confirming previous inferences that global climate influenced erosion rates (Shuster et al., 2005; Zhang et al., 2001). The apparent invariance of global weathering rates over the last 10 Ma (Willenbring and von Blanckenburg, 2010) might then indicate that physical erosion fluctuations during glacial times can be decoupled from weathering changes.

In addition, our record suggests a decrease of erosion rates after 1.7 Ma possibly suggesting that the erosional response to the onset of glaciations in the Quaternary would have been transient. This transient impact of climate on erosion is questionable at this point because there is only a limited number of data over the last 2 Ma. The large amplitude of the 100 ka glacial cycles, which appeared after 1.8 Ma, could in particular have produced a high frequency variability of the erosion signal. Therefore, we cannot exclude that the 3 younger samples of our record (at 1.58 Ma, 15 ka and present-day river sands) might fortuitously coincide with periods of low erosion. If true, this reduction in erosion observed after 1.7 Ma would only reflect a sampling bias. However, the probability of such a systematic observational artifact is low considering that interglacial periods have a short duration (<20 ka). In addition Shuster et al. (2005) have presented a thermochronometric record from the Coast Mountains suggesting a similar transient increase in erosion. Such a transient augmentation of erosion could make sense at a global scale. Indeed, under constant tectonic forcing and climate, the topography of an uplifting range is supposed to reach a steady state in which the sediment flux balances crustal shortening (Whipple and Meade, 2006). If the shortening rate across the orogeny is assumed constant while climate changes, it may cause enhanced physical erosion, leading to a transient disequilibrium until the balance between erosion and tectonic is restored back. Whipple and Meade (2006) provide simulations showing such a transient adjustment within the framework of the critical wedge theory. The time needed for this adjustment is probably scale dependent and must depend on the factors which govern isostatic rebound (i.e., the mechanical properties

Table 1
^{10}Be data. Abbreviations are: t_d, depositional age; Δt_d, the minimum and maximum ages of the reference polarity chron in which the sample falls; A_r, the accumulation rate at the time of deposition; N_a (1σ), the ^{10}Be concentration measured in the sample and its 1σ analytical uncertainty, respectively; N_s(1σ), the post-accumulation correction and its 1σ uncertainty, respectively; ε and Δε, paleo-erosion rate and its uncertainty, respectively.

Sample	t_d (Ma)	Δt_d		Ar	N_a (at.g^{-1})	1σ (N_a)	N_s (at.g^{-1})*	1σ (N_s)		N_a/N_s	ε (m/Myr)	Δε (mm/yr)	
		+	−					+	−			+	−
Kuitun section													
TF500	8.80	0.298	0.03	0.027	3.46E+03	9.1E+02	353	55	53	9.80	112	61	68
TF400	7.72	0.390	0.02	0.030	4.82E+03	7.6E+02	553	116	109	8.72	140	52	27
KBe1	5.88	0.154	0.64	0.023	3.23E+03	7.8E+02	1702	246	238	1.90	985	1059	417
TF200	5.60	0.430	0.37	0.023	7.29E+03	1.2E+03	1955	282	273	3.73	324	113	76
KBe3	5.34	0.696	0.10	0.023	1.32E+04	1.8E+03	2234	353	338	5.93	179	50	34
KBe4	4.97	0.262	0.17	0.015	7.19E+03	8.4E+02	3722	523	508	1.93	682	281	208
KBe5	4.63	0.007	0.13	0.020	9.22E+03	1.3E+03	3579	528	509	2.58	500	173	129
KBe6	4.18	0.01	0.60	0.019	1.34E+04	1.8E+03	4594	674	651	2.91	399	128	96
KBe7	3.73	0.453	0.14	0.019	1.54E+04	1.6E+03	5767	812	788	2.68	455	121	103
KBe8	3.43	0.161	0.10	0.021	1.16E+04	1.3E+03	5682	811	785	2.03	868	309	254
KBe9	3.28	0.051	0.07	0.042	2.15E+04	1.8E+03	6141	879	864	3.5	360	67	67
KBe10	3.09	0.028	0.06	0.023**	1.07E+04	1.1E+03	6755	982	949	1.59	1544	810	612
KBe11	2.72	0.316	0.13	0.023**	1.82E+04	1.8E+03	8135	1218	1198	2.23	729	210	188
KBe12	2.07	0.508	0.13	0.023**	1.25E+04	1.9E+03	11213	1591	1540	1.12	7660	38498	13537
KBe13	1.99	N/A	N/A	0.023**	1.58E+04	2.0E+03	11697	1691	1634	1.35	2535	2836	1483
KBe14	1.68	N/A	N/A	0.023**	2.09E+04	1.8E+03	13655	1940	1878	1.53	1701	896	700
KBe15	1.57	N/A	N/A	0.023**	3.95E+04	4.6E+03	14401	1880	1842	2.74	516	143	122
Terrace													
TP	0.015	N/A	N/A	N/A	1.10E+05	6.62E+03	N/A	N/A	N/A	N/A	255	30	31
River bed													
RS1	0.00	N/A	N/A	N/A	4.84E+04	2.14E+04	N/A	N/A	N/A	N/A	587	469	190
RS2	0.00	N/A	N/A	N/A	5.15E+04	1.15E+04	N/A	N/A	N/A	N/A	552	169	116
RS3	0.00	N/A	N/A	N/A	4.12E+04	6.06E+03	N/A	N/A	N/A	N/A	689	140	114

In the Xiyu conglomeratic formation (above ~500 m in thickness) the paleomagnetic sampling density was lower which yielded large uncertainties on the accumulation rates at the time of deposition. Therefore, for samples KBe10 to KBe15, we estimated their ages and erosion rates based on average accumulation rates found in the lower part of the section.
* Includes 15 at/gr due to the recent exposure at surface, N/A: non-applicable.
** Average accumulation rates.

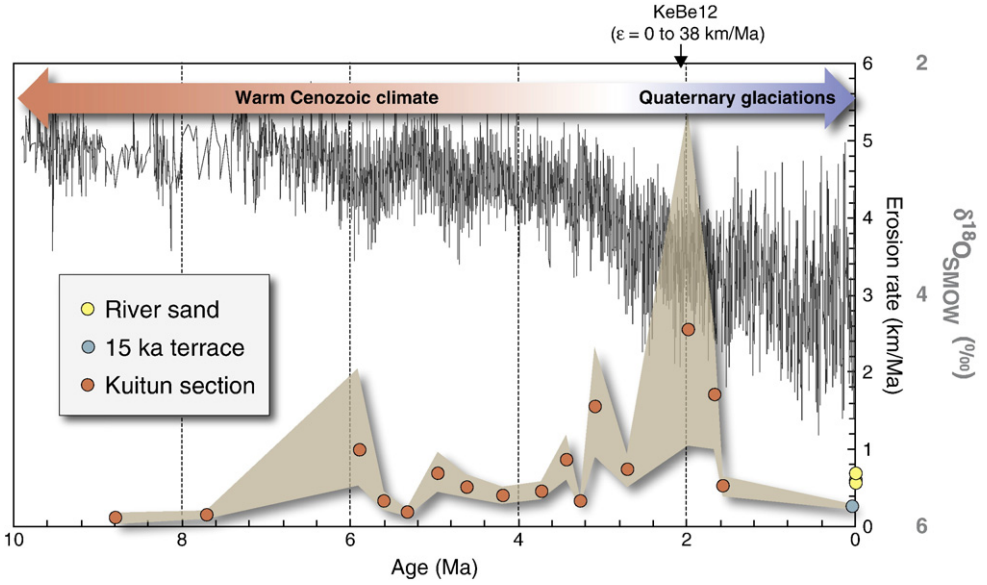

Fig. 5. Erosion rates as function of depositional age (Charreau et al., 2005) and global deep-sea oxygen isotope record (Zachos et al., 2001) over the last 10 Myr. The 1 σ uncertainty envelop is shown in gray. Sample KeBe12 is not shown because it presents very large uncertainties, but its low ^{10}Be concentration nevertheless suggests high erosion rates.

of the crust, lithosphere an asthenosphere), as well as on the erodability of exhumed rocks under fluvial and hillslope processes. Our study suggests that in the case of North Tianshan, the erosional response to the onset of Quaternary glaciations (at about 3 Ma) might thus have lasted less than 2 Ma only.

However, this scenario could also be criticized because if tectonic is constant while erosion increases, this would actually imply a reduction of the watershed altitude. This might affect the accuracy of the erosion rates that we compute here under the assumption of a constant hypsometry. However, given that the eroded material is partially balanced by isostatic and tectonic inflows, the total net altitudinal change due to enhanced erosion is probably already accounted in our uncertainties. Moreover, if true, a decreasing altitude should have lowered the production rate and yield lower cosmogenic ^{10}Be concentrations while since ~2 Ma we observe higher concentrations (Table 1). As Shuster et al. (2005), we suggest that the onset of glaciations implied a shift from fluvial to glacial erosion processes (typically V-shape to U-shape valleys) which yield to enhanced erosion. After ~2 Ma, most of the surplus material has been removed, leading to more stable U-shape glaciated valley and, then, a new equilibrium with lower erosion rates.

Finally, as this record is only focused on one single drainage basin, a limitation of this study is that the Kuitun river watershed could have been impacted by local tectonic particularities. It must also be considered that the erosion rates of Central Asia could also be partially decoupled from the global erosion rates, because of superimposed regional tectonic or local climatic particularities. Consequently, we acknowledge that the debate remains open and that this apparent transient response of erosion to climate must be tested in the future by applying this method to other localities of Central Asia and other regions of the world.

In any case our study presents a new and quite powerful approach to obtain quantitative estimates of paleo-erosion rates. It moreover provides the first record of long term erosion in a region where, as pointed out by Molnar (2004), the mass transfer is only driven by the competition between tectonics and climate and not altered by sea level changes and exposure of continental platforms.

Acknowledgements

This study was financed by the French INSU/CNRS programs SYSTER and ANR. We thank Peter Molnar and one anonymous reviewer for their very constructive comments that greatly improved the manuscript. Fruitful discussions with Jérôme Lavé and Raphaël Pik were useful for interpreting this record. Expert Jean-Pierre Valet and Yves Gallet are also thanked for their advice about the long term variations in the earth virtual magnetic moment. We are also grateful to Robert Joussemet (STEVAL mineral processing pilot plant, Lem, Nancy) for his help in separating quartz and to the ASTER team for the cosmogenic nuclide concentration measurements (M. Arnold, G. Aumaître, K. Keddadouche, L. Léanni and F. Chauvet). ASTER AMS national facility (CEREGE, Aix en Provence) is supported by the INSU/CNRS, the French Ministry of Research and Higher Education, IRD and CEA. This is CRPG contribution n° 2101.

References

Abdrakhmatov, K.Y., Aldazhanov, S.A., Hager, B.H., Hamburger, M.W., Herring, T.A., Kalabaev, K.B., Makarov, V.I., Molnar, P., Panasyuk, S.V., Prilepin, M.T., Reilinger, R.E., Sadybakasov, I.S., Souter, B.J., Trapeznikov, Y.A., Tsurkov, V.Y., Zubovich, A.V., 1996. Relatively recent construction of the Tien Shan inferred from GPS measurements crustal deformation rates. Nature 384, 450–453.

Amidon, W., Farley, K.A., 2011. Cosmogenic 3He production rates in apatite, zircon and pyroxene inferred from Bonneville flood erosional surfaces. Quaternary Geochronology 6 (1), 10–21. doi:10.1016/j.quageo.2010.03.005.

Avouac, J.-P., Burov, E.B., 1996. Erosion as a driving mechanism of intracontinental mountain growth. J. Geophys. Res. 101, 17747.

Avouac, J.-P., Tapponnier, P., Bai, P., You, M., Wang, G.A., 1993. Active thrusting and folding along the northern Tien Shan and late Cenozoic rotation of the Tarim relative to Dzungaria and Kazakhstan. J. Geophys. Res. 98, 6755–6804.

Balco, G., Stone, J.O., Lifton, N.A., Dunai, T.J., 2008. A complete and easily accessible means of calculating surface exposure ages or erosion rates from ^{10}Be and ^{26}Al measurements. Quat. Geochronol. 3, 174–195.

Berner, R.A., Lasaga, A.C., Garrels, R.M., 1983. The carbonate–silicate geochemical cycle and its effect on atmospheric carbon dioxide over the last 100 million years. Am. J. Sci. 205, 641–683.

Biggin, A.J., Strik, G.H.M.A., Langereis, C.G., 2009. The intensity of the geomagnetic field in the late-Archaean: new measurements and an analysis of the updated IAGA palaeointensity database. Earth Planet. Space 61, 9–22.

Blard, P.H., Bourles, D., Lave, J., Pik, R., 2006. Applications of ancient cosmic-ray exposures: theory, techniques and limitations. Quat. Geochronol. 1, 59–73.

Braucher, R., Bourlès, D.L., Brown, E.T., Colin, F., Muller, J.-P., Braun, J.-J., Delaune, M., Minko, A.E., Lescouet, C., Raisbeck, G.M., Yiou, F., 2000. Application of in situ-produced cosmogenic 10Be and 26Al to the study of lateritic soil development in tropical forest: theory and examples from Cameroon and Gabon. Chem. Geol. 170, 95–111.

Braucher, R., Brown, E.T., Bourlès, D.L., Colin, F., 2003. In situ produced ^{10}Be measurements at great depths: implications for production rates by fast muons. Earth Planet. Sci. Lett. 211, 251–258.

Brown, E.T., Edmond, J.M., Raisbeck, G.M., Yiou, F., Kurz, M.D., Brook, E.J., 1991. Examination of surface exposure ages of Antarctic moraines using in situ produced ^{10}Be And ^{26}Al. Geochim. Cosmochim. Acta 55, 2269–2283.

Brown, E.T., Stallard, R.F., Larsen, M.C., Raisbeck, G.M., Yiou, F., 1995. Denudation rates determined from the accumulation of in situ produced ^{10}Be in the Luquillo experimental forest, Puerto-Rico. Earth Planet. Sci. Lett. 129, 193–202.

Brown, E.T., Stallard, R.F., Larsen, M.C., Bourles, D.L., Raisbeck, G.M., Yiou, F., 1998. Determination of predevelopment denudation rates of an agricultural watershed (Cayaguas River, Puerto Rico) using in-situ-produced Be-10 in river-borne quartz. Earth Planet. Sci. Lett. 160, 723–728.

Bullen, M.E., Burbank, D.W., Garver, J.I., Abdrakhmatov, K.Y., 2001. Late Cenozoic tectonic evolution of the northwestern Tien Shan: new age estimates for the initiation of mountain building. Bull. Geol. Soc. Am. 113, 1544–1559.

Bullen, M.E., Burbank, D.W., Garver, J.I., 2003. Building the Northern Tien Shan: integrated thermal, structural, and topographic constraints. J. Geol. 111, 149–165.

Burtman, V.S., 1975. Structural geology of the Variscan Tian Shan, USSR. Am. J. Sci. 275-A, 157–186.

Chamberlain, C.P., Poage, M.A., 2000. Reconstructing the paleotopography of mountain belts from isotopic composition of authigenic minerals. Geology 28, 115–118.

Charreau, J., 2005. Tectonic evolution of the Tianshan mountains during Cenozoic time in response to the India–Asia collision: from magnetostratigraphy and U–Th/He thermochronology analysis of Neogene sediments: Orleans, Orleans.

Charreau, J., Chen, Y., Gilder, S., Dominguez, S., Avouac, J.-P., Sevket, S., Sun, D., Li, Y., Wang, W.-M., 2005. Magnetostratigraphy and rock magnetism of the Neogene Kuitun He section (northwest China): implications for Late Cenozoic uplift of the Tianshan mountains. Earth Planet. Sci. Lett. 230, 177–192.

Charreau, J., Gilder, S., Chen, Y., Dominguez, S., Avouac, J.-P., Sevket, Sen, Jolivet, M., Li, Y., Wang, W., 2006. Magnetostratigraphy of the Yaha section, Tarim Basin (China): 11 Ma acceleration in erosion and uplift of the Tianshan Mountains. Geology 34, 181–184.

Charreau, J., Avouac, J.-P., Chen, Y., Dominguez, S., Gilder, S., 2008. Miocene to present kinematics of fault-bend folding across the Huerguosi anticline, northern Tianshan (China), derived from structural, seismic, and magnetostratigraphic data. Geology 871–874.

Charreau, J., Chen, Y., Gilder, S., Barrier, L., Dominguez, S., Augier, R., Sen, S., Avouac, J.-P., Gallaud, A., Graveleau, F., Li, Y., 2009a. Neogene uplift pulses of the Tianshan mountains observed in the magnetic record of the Jingou River section (Northwest China). Tectonics 28, doi:10.1029/2007TC002137.

Charreau, J., Gumiaux, C., Avouac, J.-P., Augier, R., Chen, Y., Barrier, L., Gilder, S., Dominguez, S., Charles, N., Wang, Q., 2009b. The Neogene Xiyu Formation, a diachronous prograding gravel wedge at front of the Tianshan: climatic and tectonic implications. Earth Planet. Sci. Lett. 287, 283–310.

Charvet, J., Shu, L.S., Laurent-Charvet, S., 2007. Paleozoic structural and geodynamic evolution of eastern Tianshan (NW China): welding of the Tarim and Junggar plates. Episodes 30, 162–186.

Chmeleff, J., von Blanckenburg, F., Kossert, K., Jakob, D., 2010. Determination of the 10Be half-life by multicollector ICP-MS and liquid scintillation counting. Nucl. Instrum. Methods Phys. Res. Sect. B 268, 192–199.

Clift, P.D., 2006. Controls on the erosion of Cenozoic Asia and the flux of clastic sediment to the ocean. Earth Planet. Sci. Lett. 241, 571–580.

Dahlen, F.A., Suppe, J., 1988. Mechanics, growth, and erosion of mountain belts. In: Clark, S.P., Burchfiel, B.C., Suppe, J. (Eds.), Processes in Continental Lithospheric Deformation: Geological Society of America Special Paper, Volume 218, pp. 161–178.

Dumitru, T.A., Zhou, D., Chang, E.Z., Graham, S.A., Hendrix, M.S., Sobel, E.R., Caroll, A.R., 2001. Uplift, exhumation, and deformation in the Chinese Tian Shan. In: Hendrix, M.S., Davis, G.A. (Eds.), Paleozoic and Mesozoic Tectonic Evolution of Central Asia: From Continental Assembly to Intracontinental Deformation: Boulder: Colorado: Geological Society of America Memoir, 194, pp. 71–99.

Dunai, T.J., 2001. Influence of secular variation of the geomagnetic field on production rates of in situ produced cosmogenic nuclides. Earth Planet. Sci. Lett. 193, 197–212.

Dunne, J., Elmore, D., Muzikar, P., 1999. Scaling factors for the rates of production of cosmogenic nuclides for geometric shielding and attenuation at depth on sloped surfaces. Geomorphology 27, 3–11.

France-Lanord, C., Derry, L.A., 1997. Organic carbon burial forcing of the carbon cycle from Himalayan erosion. Nature 390, 65–75.

Galy, V., France-Lanord, C., Beyssac, O., Faure, P., Kudrass, H., Palhol, F., 2007. Efficient organic carbon burial in the Bengal fan sustained by the Himalayan erosional system. Nature 450, 407–410.

Gao, J., Li, M., Xiao, X., Tang, Y., He, G., 1998. Paleozoic tectonic evolution of the Tianshan Orogen, northwestern China. Tectonophysics 287, 213–231.

Hay, W.W., Sloan, J.L., Wold, C.N., 1988. Mass age distribution and composition of sediments on the ocean-floor and the global rate of sediment subduction. J. Geophy. Res. 93, 14933–14940.

Heermance, R.V., Chen, J., Burbank, D.W., Wang, C., 2007. Chronology and tectonic controls of Late Tertiary deposition in the southwestern Tian Shan foreland, NW China. Basin Res., doi:10.1111/j.1365-2117.2007.00339.x

Kent-Corson, M.L., Ritts, B.D., Charreau, J., Zhuang, G., Bovet, P.M., Graham, S.A., Chamberlain, P., 2008. Stable Isotopic Insights into Sedimentary Basin Evolution Along the Northern Tibetan Margin: Eos Trans. AGU, 89(53. Fall Meet. Suppl., Abstract T32A-01.

Korschinek, G., Bergmaier, A., Faestermann, T., Gerstmann, U.C., Knie, K., Rugel, G., Wallner, A., Dillmann, I., Dollinger, G., Lierse von Gosstomski, C., Kossert, K., Maiti, M., Poutivtsev, M., Remmert, A., 2010. A new value for the 10Be half-life by heavy-ion elastic recoil detection and liquid scintillation counting. Nucl. Instrum. Meth. 268, 187–191.

Lal, D., 1991. Cosmic ray labeling of erosion surfaces: in situ nuclide production rates and erosion models. Earth Planet. Sci. Lett. 104, 424–439.

Lin, W., Faure, M., Shi, Y., Wang, Q., Li, Z., 2008. Palaeozoic tectonics of the south-western Chinese Tianshan: new insights from a structural study of the high-pressure/low-temperature metamorphic belt. Int. J. Earth Sci., doi:10.1007/s00531-008-0371-7

Lourens, L., Hilgen, F., Shackleton, N.J., Laskar, J., and Wilson, D., 2004, The Neogene Period, in Felix M. Gradstein, J.G.O., and Alan G. Smith, ed., A Geological Time Scale: London, Cambridge.

Métivier, F., 2002. On the use of sedimentation rates in deciphering global change. Geophys. Res. Lett. 29.

Métivier, F., Gaudemer, Y., 1997. Mass transfer between eastern Tien Shan and adjacent basins (central Asia): constraints on regional tectonics. Geophys. J. Int. 128, 1–17.

Molnar, P., 2004. Late Cenozoic increase in accumulation rates of terrestrial sediment: how might climate change have affected erosion rates? Annu. Rev. Earth Planet. Sci. 32, 67–89.

Molnar, P., Brown, E.T., Burchfiel, B.C., Deng, Q., Feng, X., Li, J., Raisbeck, G.M., Shi, J., Wu, Z., Yiou, F., You, H., 1994. Quaternary climate change and the formation of river terraces across growing anticlines on the north flank of the Tien Shan, China. J. Geol. 102, 583–602.

Nishiizumi, K., Imamura, M., Caffee, M.W., Southon, J.R., Finkel, R.C., McAninch, J., 2007. Absolute calibration of ^{10}Be AMS standards. Nucl. Instrum. Methods Phys. Res. Sect. B 258, 403–413.

Poisson, B., Avouac, J.P., 2004. Holocene hydrological changes inferred from alluvial stream entrenchment in North Tian Shan (Northwestern China). J. Geol. 112, 231–249.

Raymo, M.E., Ruddiman, W.F., 1992. Tectonic forcing of late cenozoic climate. Nature 359, 117–122.

Refsnider, K.A., 2010, Dramatic increase in late Cenozoic alpine erosion rates recoreded by cave sediment in the southern Rocky Moutains. Earth Planet. Sci. Lett. 297, 505–511.

Reigber, C., Michel, G.W., Galas, R., Angermann, D., Klotz, J., Chen, J.Y., Papschev, A., Arslanov, R., Tzurkov, V.E., Ishanov, M.C., 2001. New space geodetic constraints on the distribution of deformation in the Central Asia. Earth Planet. Sci. Lett. 191, 157–165.

Sadler, P.M., 1999. The influence of hiatuses on sediment accumulation rates. GeoResearch Forum 5, 15–40.

Schaller, M., von Blanckenburg, F., Veldkamp, A., Tebbens, L.A., Hovius, N., Kubik, P.W., 2002. A 30 000 yr record of erosion rates from cosmogenic ^{10}Be in Middle European river terraces. Earth Planet. Sci. Lett. 204, 307–320.

Shuster, D.L., Ehlers, T.A., Rusmore, M.E., Farley, K.A., 2005. Rapid glacial erosion at 1.8 Ma revealed by 4He/3He thermochronometry. Science 310, 1668–1670.

Sobel, E.R., Dumitru, T.A., 1997. Thrusting and exhumation around the margins of the western Tarim basin during India–Asia collision. J. Geophys. Res. 102, 5043–5063.

Sobel, E., Chen, J., Heermance, R.V., 2006. Late Oligocene–Early Miocene initiation of shortening in the Southwestern Chinese Tian Shan: implications for Neogene shortening rate variations. Earth Planet. Sci. Lett. 247, 70–81.

Stone, J.O., 2000. Air pressure and cosmogenic isotope production. J. Geophys. Res. Solid Earth 105, 23753–23759.

von Blanckenburg, F., 2005. The control mechanisms of erosion and weathering at basin scale from cosmogenic nuclides in river sediment. Earth Planet. Sci. Lett. 237, 462–479.

Wang, Y., Kromhout, E., Zhang, C., Xu, Y., Parker, W., Deng, T., Qiu, Z., 2008. Stable isotopic variations in modern herbivore tooth enamel, plants and water on the Tibetan Plateau: implications of paleoclimate and paleoelevation reconstructions. Palaeogeogr. Palaeoclimatol. Palaeoecol. 260, 359–374.

Whipple, K.X., Meade, B.J., 2006. Orogen response to changes in climatic and tectonic forcing. Earth Planet. Sci. Lett. 243, 218–228.

Willenbring, J.K., von Blanckenburg, F., 2010. Long-term stability of global erosion rates and weathering during late-Cenozoic cooling. Nature 465, 211–214.

Willett, S.D., Brandon, M.T., 2002. On steady state in mountain belts. Geology 30, 175–178.

Windley, B.F., Allen, M.B., Zhang, C., Zhao, Z.-Y., Wang, G.R., 1990. Paleozoic accretion and Cenozoic deformation of the Chinese Tien Shan Range, central Asia. Geology 18, 128–131.

Yin, A., Nie, S., Craig, P., Harrison, T.M., 1998. Late Cenozoic tectonic evolution of the southern Chinese Tian Shan. Tectonics 17, 1–27.

Zachos, J., Pagani, M., Sloan, L., Thomas, E., Billups, K., 2001. Trends, rhythms, and aberrations in global climate 65 Ma to present. Science 292, 686–693.

Zeitler, P.K., Koons, P.O., Bishop, M.P., Chamberlain, C.P., Craw, D., Edwards, M.A., Hamidullah, S., Jan, M.Q., Khan, M.A., Khattak, M.U.K., Kidd, W.S.F., Mackie, R.L., Meltzer, A.S., Park, S.K., Pecher, A., Poage, M.A., Sarker, G., Schneider, D.A., Seeber, L., Shroder, J.F., 2001. Crustal reworking at Nanga Parbat, Pakistan: metamorphic consequences of thermal–mechanical coupling facilitated by erosion. Tectonics 20, 712–728.

Zhang, P., Molnar, P., Downs, W.R., 2001. Increased sedimentation rates and grain sizes 2–4 Myr ago due to the influence of climate change on erosion rates. Nature 410, 891–897.